PORE MICROSTRUCTURE CHARACTERIZATION OF Zn2SnO4 USING MERCURY INTRUSION POROSIMETRY

Tamara Ivetić[1], Jugoslav Krstić[2], Nina Finčur[3], Biljana Abramović[3], Svetlana Lukić-Petrović[1]

[1]*University of Novi Sad, Faculty of Sciences, Department of Physics, Trg Dositeja Obradovića 4, 21000 Novi Sad, Serbia*
[2]*University of Belgrade, Institute of Chemistry, Technology and Metallurgy, Department of Catalysis and Chemical Engineering, Njegoševa 12, 11000 Belgrade, Serbia*
[3]*University of Novi Sad, Faculty of Sciences, Department of Chemistry, Biochemistry and Environmental Protection, Trg Dositeja Obradovića 3, 21000 Novi Sad, Serbia*
e-mail: tamara.ivetic@df.uns.ac.rs

Abstract

The zinc stannate (Zn_2SnO_4) is marked as a promising semiconductor material to be used in a field of environmental protection and photocatalysis especially when its band gap is adjusted to enough narrow value to provide its applicability under the visible light irradiation. A traditional solid-state procedure was used to synthesize Zn_2SnO_4 when a stoichiometrical mixture of starting zinc oxide (ZnO) and tin oxide (SnO_2) powders where mechanochemically activated by grinding in a planetary ball mill for 160 min and additionally annealed at 1200°C for 2 h. In this paper, we investigate the most important textural features of the Zn_2SnO_4 powder for its usage in the photocatalytic degradation of the organic pollutants from wastewaters. Mercury intrusion porosimetry was combined with the scanning electron microscopy to study morphology and surface properties, like specific pore volume, specific surface area, apparent density, and total porosity.

Introduction

Ternary zinc-tin-oxide (Zn_2SnO_4) is a well-known *n*-type semiconductor with promising applications, like in gas sensors [1], dye-sensitized solar cells [2,3], lithium-ion batteries [4], and recently in the photocatalysis [5-9]. The photocatalytic activity of an oxide semiconductor is highly dependent on its particle size, morphology, and surface properties since photocatalytic reactions mainly occur on the catalyst surface [10]. Solid-state mechanochemistry is a simple, sustainable and economical/eco-friendly method that successfully competes against the most common multistep toxic-organic-solvent-based routes like sol-gel, hydrothermal, co-precipitation, for the synthesis of Zn_2SnO_4 [11,12]. In this work, we describe the characterization of the textural Zn_2SnO_4 powder features by mercury intrusion porosimetry assisted with the scanning electron microscopy (SEM) measurements. The results should indicate the size of the impact that surfaces' properties of the cubic Zn_2SnO_4 powder, synthesized by the mechanochemical solid-state method, have on the efficiency of Zn_2SnO_4 as a photocatalyst in the degradation of the organic compounds from wastewaters [13]. The mercury intrusion porosimetry (Fig. 1a-c) is a method very often used in powder characterization. This method is based on fact that a non-wetting liquids are not being adsorbed on the surface of solids or inside their pores [14], and thereby the volume of such liquids when forced into the pores with appropriate high pressures starting from vacuum (Fig. 1a), give a sufficient information on the materials' pore structure properties. In the beginning, basically, this type of materials characterization provides a curve called the intrusion curve, *i.e.*, the plot of the intruded volume of a non-wetting liquid (in this case mercury) per sample mass unit *vs.* the applied pressure in MPa. Using obtained intrusion curve and the appropriate theoretical model of intrusion porosimetry that takes into account

the surface tension, capillary forces and pressure, the following elementary information on the samples' textural properties could be obtained: total specific cumulative pore volume (V_{tot}), total specific surface area (*SSA*), average pore diameter (D_{av}), bulk density (ρ_{bl}), apparent (real) density (ρ_{ap}) and total porosity. Porosity is defined as the ratio of the volume of void-space and total (or bulk) volume of material, including the solid and void components. There are three categories of pores according to their size: micropores (pore diameter < 2 nm), mesopores (pore diameter 2 – 50 nm) and macropores (pore diameter > 50 nm) [14], and four according to their shape (Fig. 1d). The basic principle of the intrusion porosimetry states that the pressure required to force a non-wetting liquid (mercury is non-wetting to most solid materials) to enter a pore or capillary of circular cross-section is inversely proportional to the effective diameter of the capillary and directly proportional to the surface tension of the non-wetting liquid and angle of contact with the solid surface [15]. Essentially, if we assume that the pores or capillaries in the sample are cylindrical and circular in cross-section openings, the relationship between the applied pressure and the minimum pore size into which the non-wetting liquid will be forced to enter could be simply described by Washburn's equation [15]:

$$D = \frac{-4\gamma\,cos\theta}{P} \qquad (1)$$

where *D* is the diameter of the pore where non-wetting liquid intrudes, γ is the surface tension of the non-wetting liquid (for mercury generally 480 mN/m) and θ is the contact angle of the non-wetting liquid on the surface of a sample (for mercury generally 140 °). Therefore, the size of the pore where non-wetting liquid, like mercury, intrudes is inversely proportional to the applied pressure. Mercury intrusion porosimetry, in fact, measures the entrance towards a pore (Fig. 1e) and not the actual inner size of a pore [16], and that is the most important limitation of this technique. All this means that for any pressure it can be determined which pore sizes have been invaded by mercury and which size have not [15], so closed pores could not be analyzed since the mercury has no way of entering in. However, today's various software solutions based on different assumptions' and pore models provide an overview of how the cross-linking structure between pores looks like.
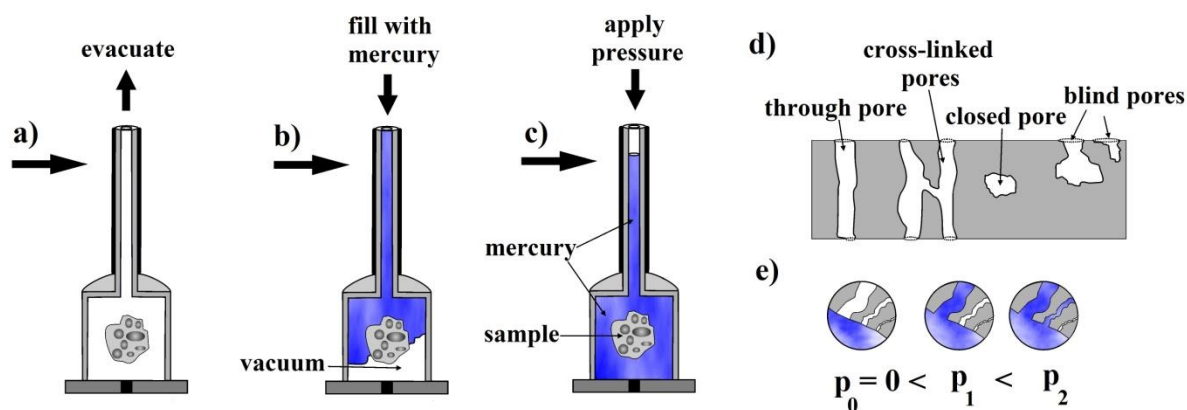

Figure 1. Schematic illustration of a)-c) mercury intrusion porosimetry principle, d) pore shape types, and e) pressures at which different pore size entrances are invaded by mercury

From the intrusion curve, the total pore volume is read as the total intruded volume of the mercury at the highest pressure determined because this property does not require Washburn's equation or a pore model. Dividing this value by mass of the sample gives the total

cumulative specific pore volume (V_{tot}) in units of volume per unit mass (cm^3/g). The total pore specific surface area is calculated by:

$$SSA = \frac{1}{\gamma |\cos\theta|} \int_0^{Vtot} p\, dV$$

(2)

and represents the area above the intrusion curve, while the average pore diameter (D_{av}) is then calculated as:

$$D_{av} = 4 \frac{V_{tot}}{S}$$

(3).

The D_{av} is an average pore diameter (more precisely, hydraulic pore diameter) which is calculated as the ratio of pore volume multiplied by four to pore area. Median pore diameter ($D_{50\%}$) is a diameter that corresponds to the 50% of total pore volume, i.e. the diameter for which one-half of the pore volume is found to be in larger pores and one-half is found to be in smaller pores. Apparent density (ρ_{ap}) is determined by a gas pycnometry as the difference between mercury pycnometry envelope density and amount of the helium uptake at the maximal uptake volume at the corresponding relative pressure.

Experimental

Zn_2SnO_4 powder sample was synthesized in the two-step solid-state processing, when starting materials, commercially available ZnO and SnO_2 (Sigma–Aldrich, purity 99.9%, particle size $\leq 1\mu m$) powders mixed in stoichiometrical ratio were first mechanically activated in high energy ball mill (Retsch GmbH PM100) using zirconium vial and zirconium balls of 10 mm diameter (ball to powder ratio = 10:1) in air for 160 min, and secondly annealed in furnace at 1200 °C for 2 hours. X-ray diffraction was carried out using the Philips PW 1050 instrument, with Cu K$\square_{1,2}$ radiation, and a step scan mode of 0.02°/s in an angular range $2\theta = 15\text{-}70°$. SEM (JEOL JSM-6460LV) was used to investigate the morphology of the obtained sample. The textural properties, including total cumulative volume (V_{tot}) and total specific surface area (*SSA*), were obtained using Porosimeter 2000 (Fisons Instruments) within the pressure range from 1 to 2000 bar, while bulk density was obtained with Macropore Unit 120 (Fisons Instruments). All samples were dried in an oven at 110 °C during 16 h and additionally evacuated from 90 min at room temperature prior to the analysis. Two intrusion-extrusion runs, denoted as Run1 and Run2, were conducted on the same powder specimen. The recordings of the intruded Hg volume vs. applied pressure were obtained through an interface Milestone 100 Software System for PC, while Pascal Ver. 1.05 software was used for calculations.

Results and discussion

The X-ray diffraction pattern of the obtained powder sample confirmed the formation of face-centered cubic spinel Zn_2SnO_4 (JCPDS card No. 74–2184) with an average crystallite size of about 40 nm, which was in detail shown elsewhere [13].

SEM image (Fig. 2a) show that agglomeration of particles exists in Zn_2SnO_4 powder sample. Likewise, the real origin of Zn_2SnO_4 particles microstructure complexity is more clearly visible in the SEM image with higher magnification (Fig. 2b) that shows octahedral shaped neck-associated and blinded Zn_2SnO_4 grains, with the sizes that vary in the range from 536 nm to 2.03 µm. This means that the real particle sizes are actually bigger than the values shown in Fig. 2b. This type of morphology is the result of reaction-sintering and grain-growth processes happening in the mechanochemically activated $ZnO\text{-}SnO_2$ system at such a high temperature (1200 °C) of synthesis.
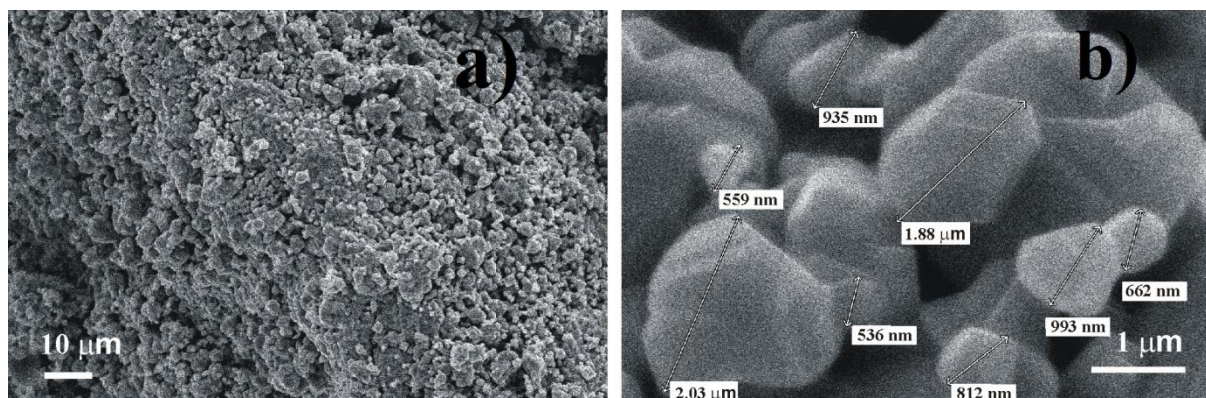
Figure 2. SEM images of Zn_2SnO_4 with different magnifications

Results obtained by the mercury intrusion porosimetry were summarized in Table 1 and revealed that the pores in Zn_2SnO_4 powder sample belong to the group of macropores (pore diameter > 50 nm). Most of the porosity comes from the intraparticle volume. The intraparticle porosity is probably a result of Zn_2SnO_4 solid-state synthesis mechanism. The expansion of the powders occurs during the solid-state reaction between the ZnO and SnO_2 particles as they are being separated when the reaction product (Zn_2SnO_4), that grows as the grain-neck region, is formed at the starting particles (ZnO and SnO_2) contact points. The voids (interparticle porosity) are only 23% of the total imprinted volume (37 mm^3 of 160 mm^3). Apparent density (ρ_{ap}) obtained from helium pycnometry is 6.13 g/cm^3 at the maximum of the applied intrusion pressure. Apparent density represents the actual density in the case of an idyllic non-porous specimen or sample with exclusively pore greater than 7.5 nm, which is the case with the obtained Zn_2SnO_4 powder sample.

Table 1. Results obtained from mercury intrusion porosimetry

Zn_2SnO_4	Run1	Run2
Total cumulative volume, V_{tot} (cm^3/g)	0.160	0.123
Total specific surface area, SSA (m^2/g)	0.31	0.27
Average pore diameter, D_{av} (μm)	2.04	1.83
Median pore diameter, $D_{50\%}$ (μm)	4.72	3.57
Total porosity (%)	49.6	43.0

The low specific surface area (Table 1) is mostly the result of mentioned Zn_2SnO_4 reaction-sintering mechanism and grain-growth at 1200 °C that causes the formation of bigger and complex particles (Fig. 2b) but also the agglomeration is noticed as well (Fig. 2a). This all may be the main reason for the inefficient photocatalytic performance of the obtained Zn_2SnO_4 powder sample when used for degradation of alprazolam, short-acting anxiolytic of the benzodiazepine class of psychoactive drugs [13] because a large surface area is desirable for the efficient photocatalysis.

Conclusion
In this paper, we report the textural properties of the solid-state synthesized Zn_2SnO_4 powder using mercury intrusion porosimetry. The data obtained using this technique and combined with the SEM images pointed out that mechanism of the solid-state Zn_2SnO_4 reaction synthesis defines its textural properties and contributes to its poor photocatalytic performance in the degradation of some pharmaceutically active compounds from wastewaters.

Acknowledgments

References

[1] W. Wang, H. Chai, X. Wang, X. Hu, X. Li, Appl. Surf. Sci. 341 (2015) 43.

[2] B. Tan, E. Toman, Y. Li, Y. Wu, J. Am. Chem. Soc. 129 (2007) 4162.

[3] K. Wang, Y. Shi, W. Guo, X. Yu, T. Ma, Electrochim. Acta 135 (2014) 242.

[4] L. Qin, S. Liang, A. Pan, X. Tan, Mater. Lett. 141 (2015) 255.

[5] M.B. Ali, F. Barka–Bouaifel, H. Elhouichet, B. Sieber, A. Addad, L. Boussekey, M. Férid, R. Boukherrab, J. Colloid Interf. Sci. 457 (2015) 360.

[6] E.L. Foletto, J.M. Simões, M.A. Mazutti, S.L. Jahn, E.I. Muller, L.S.F. Pereira, E.M. de Morales Flores, Ceram. Int. 39 (2013) 4569.

[7] L. Shi, Y. Dai, J. Mater. Chem. A 1 (2013) 12981.

[8] T. Jia, J. Zhao, F. Fu, Z. Deng, W. Wang, Z. Fu, F. Meng, Int. J. Photoenergy 2014 (2014) 197824.

[9] S. Baruah, J. Dutta, Sci. Technol. Adv. Mater. 12 (2011) 013004.

[10] T.B. Ivetić, M.R. Dimitrievska, N.L. Finčur, Lj.R. Đačanin, I.O. Gúth, B.F. Abramović, S.R. Lukić-Petrović, Ceram. Int. 40 (2014) 1545.

[11] K. Ralphs, C. Hardacre, S.L. James, Chem. Soc. Rev. 42 (2013) 7701.

[12] V. Šepelák, S.M. Becker, I. Bergmann, S. Indris, M. Scheuermann, A. Feldhoff, C. Kübel, M. Bruns, N. Stürzl, A.S. Ulrich, M. Ghafari, H. Hahn, C.P. Grey, K.D. Becker, P. Heitjans, J. Mater. Chem. 22 (2012) 3117.

[13] T.B. Ivetić, N.L. Finčur, Lj.R. Đačanin, B.F. Abramović, S.R. Lukić–Petrović, Mater. Res. Bull. 62 (2015) 114.

[14] S. Westermarck, Use of Mercury porosimetry and nitrogen adsorption in characterization of the pore structure of mannitol and microcrystalline cellulose powders, granules and tablets, Academic Dissertation, Helsinki, 2000, p. 1-60.

[15] P.A. Webb, An introduction to the physical characterization of materials by mercury intrusion porosimetry with emphasis on reduction and presentation of experimental data, Micrometrics Instrument Corp., Norcross, Georgia, 2001, p. 1-22.

[16] H. Giesche, Part. Part. Syst. Charact. 23 (2006) 1.